arXiv:2306.04864v1 [physics.atom-ph] 8 Jun 2023

Extraction of XUV+IR ionization amplitudes from the circular dichroic phase

Anatoli S. Kheifets
Research School of Physics, The Australian National University, Canberra ACT 2601, Australia
(Dated: June 9, 2023)

A strong helicity dependence of reconstruction of attosecond bursts by beating of two-photon transitions (RABBITT) with circularly polarized XUV and IR pulses was reported by Han *et al.* [Nature Physics 19, 230 and arXiv 2302.04137 (2023)]. They attributed a circular dichroic phase in RABBITT to the helical structure of the photoelectron wave packets in the final state. We exploit this effect to determine the magnitude and phase of two-photon XUV+IR ionization amplitudes. In s-electron targets (H, He, Li), such a determination is fully *ab initio* and free from any instrumental limitations. In heavier noble gases like Ar, characterization of two-photon ionization amplitudes can be made from the circular dichroic phase with minimal and very realistic assumptions.

PACS numbers: 32.80.Rm 32.80.Fb 42.50.Hz

Circular dichroism (CD) in atomic and molecular photoionization has been studied intensely in recent years. In chiral molecules, it is attributed to the left and right handedness of molecular enantiomers [1]. In atoms, electron ring current in various magnetic sublevels can be co- or counter-rotating (CO or CR) with the circularly polarized ionizing radiation. This results in different ionization probabilities [2–4] and time delays [5]. The CD effect is inherent in atomic double photoionization where the momenta of the two receding photoelectrons and the propagation direction of the photon form a chiral triangle [6–9]. Chirality can be also imprinted on atoms by a synthetic chiral light [10]. Very recently, the CD effect has been observed in the process of reconstruction of attosecond bursts by beating of two-photon transitions (RABBITT) driven by circularly polarized radiation [11, 12]. Depending on the co- and counter-rotating of the extreme ultraviolet (XUV) pump and the infrared (IR) probe pulses, the atoms exhibited different set of RABBITT magnitude and phase parameters. This effect was attributed to the helical structure of the photoelectron wave packets in the final state. While in the CR case, absorption of an IR photon leads to the final state composed of two partial waves, the CO configuration corresponds to the final state with just a single partial wave. This disparity is responsible for the RABBITT CD effect. The same single and dual wave disparity creates a circular dichroic time delay in single XUV photon ionization [5]. However, its observation requires a polarized target atom while in RABBITT such a polarization is not necessary. The RABBITT process with linear polarization is driven by interference of the two dual wave final states and their amplitudes and phases are entangled. Disparity of the circular polarization RABBITT creates an opportunity to disentangle the two interfering final states and to extract the corresponding ionization amplitudes and phases individually. In the present work, we demonstrate such an extraction for the helium atom and show that it is free from any instrumental limitations and inaccuracies. This way a complete experiment can be performed in two-photon XUV+IR ionization similarly to single XUV photon ionization [13, 14]. In heavier noble gases like argon, the full characterization of the two-photon ionization amplitudes can be made from the circular dichroic phase using minimal and very realistic assumptions.

In a RABBITT measurement [15, 16], an ionizing XUV attosecond pulse train (APT) is superimposed on an attenuated and variably delayed replica of the driving IR pulse. The XUV photon $\Omega^{\pm} = (2q \pm 1)\omega$ is absorbed from the initial bound state and then is augmented by an IR photon absorption $+\omega$ or emission $-\omega$ leading to formation of the even order sideband (SB) in the photoelectron spectrum. The center of the IR pulse is shifted relative to the APT by a variable delay τ such that the magnitude of a SB peak oscillates as

$$S_{2q}(\tau) = A + B\cos[2\omega\tau - C] \ . \tag{1}$$

The RABBITT parameters A, B and C entering Eq. (1) can be expressed as

$$\begin{aligned} A &= \sum_m |\mathcal{M}_m^{(-)}(\boldsymbol{k})|^2 + |\mathcal{M}_m^{(+)*}(\boldsymbol{k})|^2 \\ B &= 2\mathrm{Re}\sum_m \left[\mathcal{M}_m^{(-)}(\boldsymbol{k})\mathcal{M}_m^{(+)*}(\boldsymbol{k})\right] \\ C &= \arg\sum_m \left[\mathcal{M}_m^{(-)}(\boldsymbol{k})\mathcal{M}_m^{(+)*}(\boldsymbol{k})\right] \equiv 2\omega\tau_a \ . \end{aligned} \tag{2}$$

Here $\mathcal{M}_m^{(\pm)}(\boldsymbol{k})$ are complex and angle-dependent amplitudes of two-photon ionization produced by adding $(+)$ or subtracting $(-)$ an IR photon, respectively. An incoherent summation over the angular momentum projection of the initial state m is explicit in Eq. (2). The atomic time delay τ_a quantifies the timing of the XUV ionization process.

The angular dependence of the amplitudes $\mathcal{M}^{\pm}(\boldsymbol{k})$ can be deduced from an analytic expression [17]:

$$\begin{aligned} \mathcal{M}_m^{\pm}(\boldsymbol{k}) \ \propto \ & \sum_{\lambda=l\pm1}\sum_{L=\lambda\pm1}\sum_{|M|\le L;\mu|\le\lambda} (-i)^L e^{i\eta_L} Y_{LM}(\hat{k}) \\ & \times \oint\!\!\!\!\!\!- \ d^3\kappa \ \frac{\langle R_{kL}|r|R_{\kappa\lambda}\rangle\langle R_{\kappa\lambda}|r|R_{ln}\rangle}{E_i + \Omega^{\pm} - \kappa^2/2 - i\gamma} \\ & \times \langle Y_{LM}|Y_{1m_2}|Y_{\lambda\mu}\rangle\langle Y_{\lambda\mu}|Y_{1m_1}|Y_{lm}\rangle \end{aligned} \tag{3}$$

Here $\langle nl|$, $\langle \kappa\lambda|$ and $\langle kL|$ are the initial, intermediate and final electron states defined by their linear and angular momenta. The linear polarization (the LIN case) corresponds to $m_1 = m_2 = 0$ whereas for the circular polarization $m_1 = 1$ and $m_2 = \pm 1$ in the CO/CR cases, respectively.

For an s-electron target, $l = m = 0$ and $\lambda = 1$. The LIN and CR cases correspond to $M = 0$ and $L = \{0, 2\}$ whereas the CR case has $M = 2$ which excludes $L = 0$. By carrying out the angular integration in Eq. (3) we can write

$$\mathcal{M}^{\pm}(\boldsymbol{k}) = \begin{cases} T_0^{\pm} + 2P_2(\cos\theta)T_2^{\pm} & \text{LIN} \\ -T_0^{\pm} + P_2(\cos\theta)T_2^{\pm} & \text{CR} \\ e^{2i\phi}\sin^2\theta\, T_2^{\pm} & \text{CO}\,, \end{cases} \tag{4}$$

where $T_L^{\pm}$ absorbs the radial parts of Eq. (3). In the LIN case, $\theta = 90^\circ$ defines the photon propagation direction whereas in the CO/CR cases this direction corresponds to $\theta = 0/180^\circ$. That is why to compare the linear and circular cases, we shift the CO/CR angular scale by 90°. The polar angle ϕ in Eq. (4) is immaterial because of the rotational symmetry of the ionization process. For the same reason, the directions θ and $180^\circ - \theta$ are equivalent. So only half of the azimuthal angular range needs to be analyzed.

Eq. (4) defines the RABBITT phase for $\phi = 0$:

$$\begin{aligned} C^{\rm LIN} &= \arg\left[T_2^- T_2^{+*}\right] + \\ &\arg\left[2P_2(\cos\theta) + \frac{T_0^-}{T_2^-}\right] + \arg\left[2P_2(\cos\theta) + \left(\frac{T_0^+}{T_2^+}\right)^*\right] \\ C^{\rm CR/CO} &= \arg\left[T_2^- T_2^{+*}\right] + \arg\left[P_2(\cos\theta) - \frac{T_0^{+/-}}{T_2^{+/-}}\right] \end{aligned} \tag{5}$$

We observe in Eq. (5) that the phases of the $\pm$ transition amplitudes are entangled in the LIN case whereas they stand alone in the CR/CO cases. For further analysis, we rewrite the ratio $T_0^{\pm}/T_2^{\pm} = R^{\pm}\exp(\pm i\Delta\Phi)$ and note that $R^+ < 1 < R^-$ by virtue of the Fano [18] propensity rule for the continuous-continuous (CC) transitions [19]. We also use the emission/absorption phase identity $\Delta\Phi \equiv \Phi_{L'}^- - \Phi_L^+ \approx \Phi_{L'}^{\pm} - \Phi_L^{\pm}$ postulated in [20]. Based on this identity and Eq. (5), $\Delta\Phi = C_{\rm CO}(\theta_{\rm m}) - C_{\rm CR}(\theta_{\rm m})$ where the "magic angle" defines the node of the Legendre polynomial $P_2(\theta_m) = 0$. With all these observations, we can conclude that the LIN phase is sandwiched between the CO and CR ones:

$$C_{\rm CR}(\theta) < C_{\rm LIN}(\theta) < C_{\rm CO}(\theta) \quad \forall\theta \tag{6}$$

To prove that this relation is indeed satisfied, we conduct a set of simulations by solving numerically the time-dependent Schrödinger equation which describes the helium atom driven by the RABBITT configuration of pulses. Numerical details of these simulations can be found in our recent works [21, 22]. Most essentially, the IR carrier wavelength is set in the 800 nm range and the XUV and IR field intensities are kept within 1×10^{10} W/cm^2 range. The latter condition keeps the ionization process within the boundaries of the lowest order perturbation theory (LOPT) which is used to derive Eq. (3).

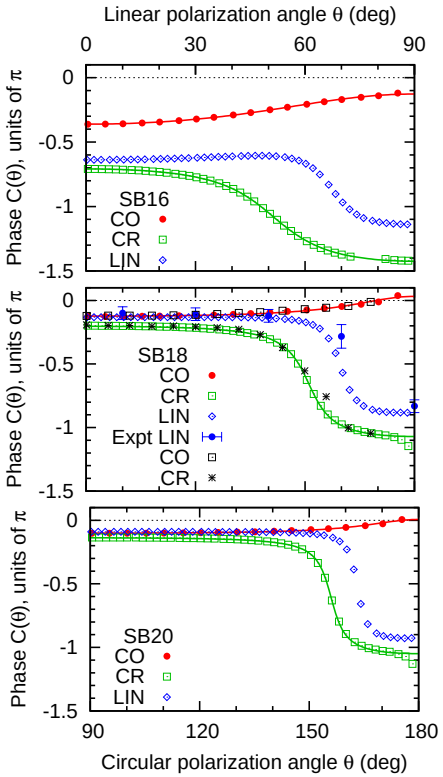


FIG. 1: Angular dependent RABBITT phase ($C(\theta)$ parameter) in SB16-20 of helium obtained with CO (red circles) and CR (green squares) circular polarization as well as with linear (LIN) polarization (blue diamonds). The CO and CR fit with Eq. (5) is shown with red and green solid lines, respectively. The experimental linear phase for SB18 is from [23] and CO/CR phases are from [12].

The results of the TDSE calculations on He are exhibited in Fig. 1 for the lowest sidenabds SB16-20. Our numerical results fully support Eq. (6) and are in good agreement with the experimental LIN phase for SB18 reported in [23]. Another important observation is that the boundaries of the CO/CR phases that encompass the LIN phase become narrower as the SB order grows. Simultaneously, the phase drop by $\sim \pi$ becomes steeper. The latter observation for the LIN phase has already been made and attributed to the convergence $R^{\pm} \to 1$ [20, 24, 25].

While the two ratios $R^{\pm}$ enter the LIN phase in Eq. (5), the CO/CR phases contain them separately. Hence, we can fit our numerical CO/CR phases with the analytic expression (5) and obtain the corresponding ratios $R^{\pm}$ and phase differences $\Delta\Phi^{\pm}$. Results of this procedure are exhibited in Fig. 2. The top panel shows the ratios $R^{\pm} = |T_0^{\pm}/T_2^{\pm}|$ whereas the bottom panel displays the phase differences $\Delta\Phi^{\pm} = \arg[T_0^{\pm}/T_2^{\pm}]$. Thus extracted ratios $R^{\pm}$ are compared with the values returned by a hydrogenic model deployed in [20]. As expected $R^{\pm} \to 1$ and $\Delta\Phi^{\pm} \to 0$ as the photoelectron energy grows. The

emisson/absorption phase identity as well as the phase determination at the magic angle are well supported by our numerical results. With our ratio determination, we can estimate an excess of the CO RABBITT magnitude over the CR one by the value of +10% for SB32 and +7% for SB34 which is very similar to [11] and contrary to [26]. The latter work claims the CR excess over the CO one.

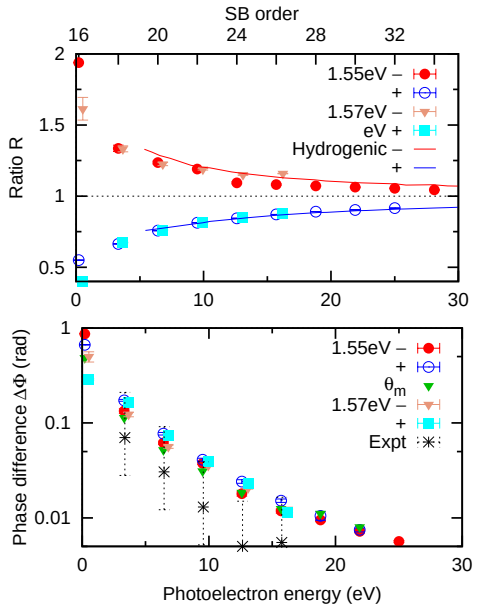


FIG. 2: Top: ratios $R^{\pm} = |T_0^{\pm}/T_2^{\pm}|$ as extracted from the fit of Eq. (5) to RABBITT phases of helium $C(\theta)$ calculated in TDSE and shown in Fig. 1. Comparison is made with a hydrogenic model employed in [20]. Bottom: the phase differences $\Delta\Phi^{\pm} = \arg[T_0^{\pm}/T_2^{\pm}]$ as extracted from the same fit as well as the magic angle difference $\Delta\Phi(\theta_{\rm m})$. The experimental values are from [12].

The hydrogenic model exploited in [17, 20] looses its validity close to threshold at very low photoelectron energies. In the present case, this model clearly fails for SB16. This sideband is formed by an IR photon absorption via an intermediate discrete bound state. Such an under-threshold (or uRABBITT) process has been studied extensively in He [27–30] and in heavier noble gases - Ne [31–33] and Ar [21]. In helium, the discrete phase Φ^+ oscillates with the IR photon energy ω when the submerged harmonic peak H15 passes through the discrete $1s3p$ level. As an illustration of this oscillation, we compare in Fig. 2 the two sets of TDSE calculations performed at the central IR frequency of 1.55 eV and 1.57 eV. Such a minuscule photon energy variation causes a significant change of the ratio and the phase difference for SB16 while these parameters for other sidebnads remain barely changed.

In p-electron targets, the parameterization of the two-photon amplitudes depends on the orbital momentum projection m. In the CO case, these m-specific amplitudes take the form:

$$\begin{aligned}
\mathcal{M}^{-}_{m=0} &\propto \cos\theta\,[-T_1^- + \bar{P}_3(\cos\theta)\,T_3^-] \\
\mathcal{M}^{+}_{m=0} &\propto e^{2i\phi}\sin^2\theta\cos\theta\,T_3^+ \\
\mathcal{M}^{-}_{m=+1} &\propto \sin\theta\,[-6T_1^- + \bar{P}_3^1(\cos\theta)\,T_3^-] \\
\mathcal{M}^{+}_{m=+1} &\propto e^{3i\phi}\sin^3\theta\,T_3^+ \\
\mathcal{M}^{\pm}_{m=-1} &\propto \mp\sin\theta\,[-T_1^{\pm} + \bar{P}_3^1(\cos\theta)\,T_3^{\pm}]
\end{aligned} \tag{7}$$

The CR amplitudes can be obtained by permutation of the emission/absorption +/− superscripts. In Eq. (7) we introduce $\bar{P}_3(\cos\theta) = P_3/P_1 = (5\cos^2\theta - 3)/2$ and $\bar{P}_3^1(\cos\theta) = P_3^1/P_1^1 = 3(5\cos^2\theta - 1)/2$.

Eq. (7) defines the RABBITT phases for $\phi = 0$:

$$\begin{aligned}
C^{\rm CR/CO}_{m=0} &= \arg\left[T_3^- T_3^{+*}\right] + \arg\left[\bar{P}_3(\cos\theta) - \frac{T_1^{\pm}}{T_3^{\pm}}\right] \\
C^{\rm CR/CO}_{m=+1} &= \arg\left[T_3^- T_3^{+*}\right] + \arg\left[\frac{1}{6}\bar{P}_3^1(\cos\theta) - \frac{T_1^{\pm}}{T_3^{\pm}}\right]
\end{aligned} \tag{8}$$

We do not present here the explicit expressions for the RABBITT phases in the $m = -1$ case for brevity. We only note that it is entangled with the $\pm$ amplitudes and that $C^{\rm CR}_{m=-1} = C^{\rm CO}_{m=-1}$. Eqs. (8) offer a convenient parameterization of the RABBITT phases for $m = 0$ and $m = +1$ in terms of the ratios $R^{\pm} = |T_1^{\pm}/T_3^{\pm}|$ and the phase differences $\Delta\Phi^{\pm} = \arg[T_1^{\pm}/T_3^{\pm}]$. We demonstrate the utility of this parameterization in Fig. 3 where we plot the RABBITT phases for the lowest SB12 in argon. The top and middle panels of this figure display the CO and CR phases, respectively, for m-resolved and m-summed cases. The ratios $R^{\pm}$ and phase differences $\Delta\Phi^{\pm}$ are used as fitting parameters to fit the corresponding CO/CR phases. These parameters are displayed in Fig. 4. Two separate fits of $m = 0$ and $m = +1$ produce the two sets of parameters which should, in principle, be identical. Their actual difference serves as an accuracy indication of the fitting procedure. We note that, similarly to helium, $R^+ < 1 < R^-$. The only exception is $R^+_{m=0}$ which exceeds unity for highest SB26-28. If this result is not accidental, it may signal a break up of the Fano propensity rule due to the proximity to the Cooper minimum where the discrete transition $3p \to Es$ gradually takes over the $3p \to Ed$.

While the individual m parameterization is very accurate and the acquired sets of the ratios and phase differences are sufficiently close between the $m = 0$ and $m = +1$ projections, such a parameterization is not practical experimentally. Indeed, a RABBITT measurement on an unpolarized target atom corresponds to the incoherent m summation. To deduce the two-photon ionization amplitude from such a measurement we analyze the CD exhibited in the bottom panel of Fig. 3. Because of the CR/CO phase identity of the $m = -1$ amplitude, its contribution vanishes from the CD. In addition, the $m = 0$ amplitude makes no contribution in the polarization plane. Thus, close to $\theta = 90°$, it is the $m = +1$ amplitude that brings the dominant contribution. This

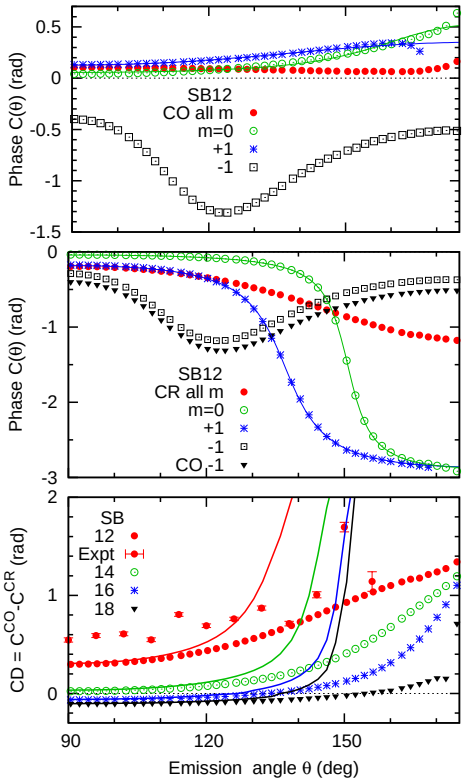


FIG. 3: Angular dependent RABBITT phase ($C(\theta)$ parameter) in SB12 of argon obtained with CO (top panel) and CR (middle panel) circular polarization. The TDSE calculations with the sum over all m projections are shown with red dots whereas m specific calculations are displayed with green circles ($m = 0$), blue asterisks ($m = 1$) and black squares ($m = -1$). The CO calculation with $m = -1$ is overplotted in the middle panel with balck triangles to demonstrate that $C^{\rm CR}_{m=-1} \simeq C^{\rm CO}_{m=-1}$. The parameterization with Eq. (5) for $m = 0$ and $m = +1$ is shown with the solid lines of the matching color. Bottom: the CD= $C^{\rm CO} - C^{\rm CR}$ for SB12-18 The dotted symbols and the solid lines of matching color correspond to the all m and $m = +1$ calculations, respectively. The experimental CD values for SB12 are from [11].

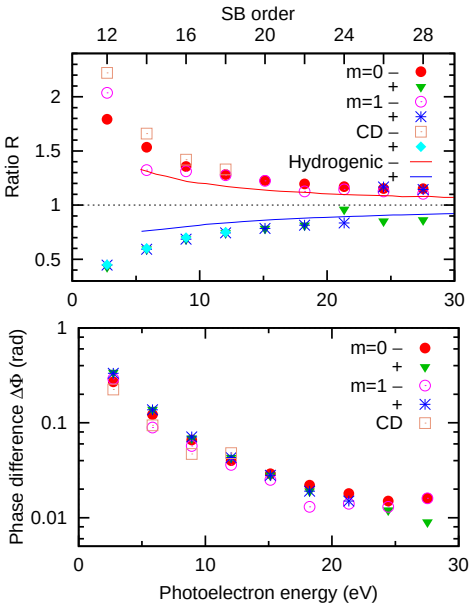


FIG. 4: Top: the ratios $R^{\pm} = |T_1^{\pm}/T_3^{\pm}|$ as extracted from the fit of Eq. (8) to RABBITT CO/CR phases with $m = 0$ and $m = +1$ as well the fit of the m-summed CD. Comparison is made with a hydrogenic model employed in [20]. Bottom: the analogous results for the phase differences $\Delta\Phi^{\pm} = \arg[T_1^{\pm}/T_3^{\pm}]$.

is illustrated in the bottom panel of Fig. 3 where the CD calculated from the $m = +1$ amplitudes and the incoherent m summation are exhibited. By using the proximity of the two sets of results near $\theta = 90°$, we apply the $m = +1$ parameterization to the m-summed CD results over a restricted angular range. Because the CD contains both the absorption and emission $\pm$ amplitudes, the number of the fitting parameters should be doubled in comparison with the separate CO and CR fits. Such an extended fit becomes unstable and we need to impose additional restrictions on the fitting parameters to improve its accuracy. To do so, we require that $R^+ = 1/R^-$ and $\Delta\Phi^+ = \Delta\Phi^-$. These restrictions are well justified as is seen from the results of the separate CO/CR fits for $m = 0$ and $m = +1$ projections. The results of the restricted R and $\Delta\Phi$ fit of the CD are overploted in Fig. 4 for the lowest SB12-18 and are found in fair agreement with the other four CR/CO and $m = 0, +1$ sets of parameters.

Similar to the helium results exhibited in Fig. 2, the hydrogenic approximation to the amplitude ratios is more or less accurate for sufficiently large photoelectron energies. However, close to the threshold, the deviation between the absorption and emission $\pm$ ratios becomes significantly larger than predicted by the hydrogenic model.

In conclusion, we devised a procedure to extract the complex two-photon ionization amplitudes from the circular dichroic phase acquired in a RABBITT measurement with circular polarized XUV and IR pulses. Such measurements have been realized very recently by Han *et al.* [11, 12] and demonstrated distinct sets of RABBITT parameters with the co- and counter-rotating XUV/IR radiations. In the case of helium and other s-electron targets, the proposed method rests solely on the experimentally accessible dichroic phase and does not require any further approximations or simplifications. Moreover, as the amplitudes are extracted from the angular dependent dichroic phase, the absolute value of the latter is not needed. This is important experimentally as this absolute value can be affected by the XUV harmonic group delay. In the case of p-electron targets such as outer shells of heavier noble gases, the amplitude extraction can be made fully *ab initio* from the m-resolved dichroic phase. In this procedure the proximity of the $m = 0$ and $m = +1$ results serves as a useful check of the accuracy of the method. In experimental measurements on unpolarized targets, the two-photon amplitudes can be extracted from the angular dependent CD taken as the difference between RABBITT phases acquired with the CO and CR circular polarizations. The CD determi-

nation of the two-photon ionization amplitudes rests on the assumption that the absorption/emission ratio and the phase difference are about the same in the CR and CO cases. This assumption is well justified by the m-specific tests of Ar.

In a broader context, our results offer an opportunity to conduct a complete experiment on the two-photon XUV+IR ionization whereupon the moduli and phases of all the relevant ionization amplitudes are determined experimentally. So far such experiments could only be conducted in single-photon XUV ionization [13, 14]. An alternative method based on the global fitting of the time- and angle-resolved RABBIT traces [31] allows to extract the two-photon amplitudes in various m-projected ionization channels [11]. However, these amplitudes are not independent and can be further reduced to the most essential "building blocks" as demonstrated in the present study. These blocks visualize very distinctly the fundamental properties of two-photon ionization such as the Fano propensity rule both for the discrete [18] and the continuous transitions [19] as well as the emisson/absorption phase identity [20]. The proposed method also tests the validity of the hydrogenic model [17, 20] which fails near the threshold and in the vicinity of resonant excitations.

Acknowledgment: Resources of the National Computational Infrastructure facility have been used in the present work.

[1] R. Cireasa, A. E. Boguslavskiy, B. Pons, M. C. H. Wong, D. Descamps, S. Petit, H. Ruf, N. Thiré, F. A., J. Suarez, et al., *Probing molecular chirality on a sub-femtosecond timescale*, Nature Physics **11**, 654 (2015).

[2] I. Barth and O. Smirnova, *Nonadiabatic tunneling in circularly polarized laser fields: Physical picture and calculations*, Phys. Rev. A **84**, 063415 (2011).

[3] I. Barth and O. Smirnova, *Spin-polarized electrons produced by strong-field ionization*, Phys. Rev. A **88**, 013401 (2013).

[4] S. Walker, L. Kolanz, J. Venzke, and A. Becker, *Selectivity in electron emission induced by ultrashort circularly polarized laser pulses*, Phys. Rev. Res. **3**, 043051 (2021).

[5] I. A. Ivanov and A. S. Kheifets, *Time delay in atomic photoionization with circularly polarized light*, Phys. Rev. A **87**, 033407 (2013).

[6] J. Berakdar and H. Klar, *Circular dichroism in double photoionization*, Phys. Rev. Lett. **69**, 1175 (1992).

[7] J. Viefhaus, L. Avaldi, G. Snell, M. Wiedenhöft, R. Hentges, A. Rüdel, F. Schäfers, D. Menke, U. Heinzmann, A. Engelns, et al., *Experimental evidence for circular dichroism in the double photoionization of helium*, Phys. Rev. Lett. **77**, 3975 (1996).

[8] V. Mergel, M. Achler, R. Dörner, K. Khayyat, T. Kambara, Y. Awaya, V. Zoran, B. Nyström, L. Spielberger, J. H. McGuire, et al., *Helicity dependence of the photon-induced three-body coulomb fragmentation of helium investigated by cold target recoil ion momentum spectroscopy*, Phys. Rev. Lett. **80**, 5301 (1998).

[9] A. S. Kheifets and I. Bray, *Calculation of circular dichroism in helium double photoionization*, Phys. Rev. Lett. **81**(21), 4588 (1998).

[10] N. Mayer, S. Patchkovskii, F. Morales, M. Ivanov, and O. Smirnova, *Imprinting chirality on atoms using synthetic chiral light fields*, Phys. Rev. Lett. **129**, 243201 (2022).

[11] M. Han, J.-B. Ji, T. Balciunas, K. Ueda, and H. J. Wörner, *Attosecond circular-dichroism chronoscopy of electron vortices*, Nature Physics **19**, 230 (2023).

[12] M. Han, J.-B. Ji, L. C. Sum, K. Ueda, and H. J. Wörner, *Separation of Wigner and continuum-continuum delays by mirror-symmetry-broken attosecond interferometry*, arXiv 2302.04137 (2023).

[13] E. Shigemasa, J. Adachi, K. Soejima, N. Watanabe, A. Yagishita, and N. A. Cherepkov, *Direct determination of partial wave contributions in the σ^* shape resonance of co molecules*, Phys. Rev. Lett. **80**, 1622 (1998).

[14] Z.-M. Wang and D. S. Elliott, *Determination of cross sections and continuum phases of rubidium through complete measurements of atomic multiphoton ionization*, Phys. Rev. Lett. **84**, 3795 (2000).

[15] P. M. Paul, E. S. Toma, P. Breger, G. Mullot, F. Augé, P. Balcou, H. G. Muller, and P. Agostini, *Observation of a train of attosecond pulses from high harmonic generation*, Science **292**(5522), 1689 (2001).

[16] Y. Mairesse, A. de Bohan, L. J. Frasinski, H. Merdji, L. C. Dinu, P. Monchicourt, P. Breger, M. Kovacev, R. Taïeb, B. Carré, et al., *Attosecond synchronization of high-harmonic soft x-rays*, Science **302**(5650), 1540 (2003).

[17] J. M. Dahlström *et al*, *Theory of attosecond delays in laser-assisted photoionization*, Chem. Phys. **414**, 53 (2013).

[18] U. Fano, *Propensity rules: An analytical approach*, Phys. Rev. A **32**, 617 (1985).

[19] D. Busto, J. Vinbladh, S. Zhong, M. Isinger, S. Nandi, S. Maclot, P. Johnsson, M. Gisselbrecht, A. L'Huillier, E. Lindroth, et al., *Fano's propensity rule in angle-resolved attosecond pump-probe photoionization*, Phys. Rev. Lett. **123**, 133201 (2019).

[20] D. I. R. Boll, L. Martini, A. Palacios, and O. A. Fojón, *Two-color polarization control of angularly resolved attosecond time delays*, Phys. Rev. A **107**, 043113 (2023).

[21] A. S. Kheifets, *Under-threshold RABBITT in argon*, J. Phys. B **56**(9), 095201 (2023).

[22] A. S. Kheifets and Z. Xu, *Polarization control of RABBITT in noble gas atoms* (2023), arXiv 2304.13889.

[23] W. Jiang, G. S. J. Armstrong, J. Tong, Y. Xu, Z. Zuo, J. Qiang, P. Lu, D. D. A. Clarke, J. Benda, A. Fleischer, et al., *Atomic partial wave meter by attosecond coincidence metrology*, Nature Communications **13**, 5072 (2022).

[24] S. Heuser, A. Jiménez Galán, C. Cirelli, C. Marante, M. Sabbar, R. Boge, M. Lucchini, L. Gallmann, I. Ivanov, A. S. Kheifets, et al., *Angular dependence of photoemission time delay in helium*, Phys. Rev. A **94**, 063409 (2016).

[25] I. A. Ivanov and A. S. Kheifets, *Angle-dependent time*

delay in two-color XUV+IR photoemission of He and Ne, Phys. Rev. A **96**, 013408 (2017).

[26] T. Mazza, M. Ilchen, A. J. Rafipoor, C. Callegari, P. Finetti, O. Plekan, K. C. Prince, R. Richter, M. B. Danailov, A. Demidovich, et al., *Determining the polarization state of an extreme ultraviolet free-electron laser beam using atomic circular dichroism*, Nature Communications **5**, 3648 (2014).

[27] M. Swoboda, T. Fordell, K. Klünder, J. M. Dahlström, M. Miranda, C. Buth, K. J. Schafer, J. Mauritsson, A. L'Huillier, and M. Gisselbrecht, *Phase measurement of resonant two-photon ionization in helium*, Phys. Rev. Lett. **104**, 103003 (2010).

[28] L. Drescher, T. Witting, O. Kornilov, and M. J. J. Vrakking, *Phase dependence of resonant and antiresonant two-photon excitations*, Phys. Rev. A **105**, L011101 (2022).

[29] L. Neoričić, D. Busto, H. Laurell, R. Weissenbilder, M. Ammitzböll, S. Luo, J. Peschel, H. Wikmark, J. Lahl, S. Maclot, et al., *Resonant two-photon ionization of helium atoms studied by attosecond interferometry*, Frontiers in Physics **10** (2022).

[30] A. Autuori, D. Platzer, M. Lejman, G. Gallician, L. Maëder, A. Covolo, L. Bosse, M. Dalui, D. Bresteau, J.-F. Hergott, et al., *Anisotropic dynamics of two-photon ionization: An attosecond movie of photoemission*, Science Advances **8**(12), eabl7594 (2022).

[31] D. M. Villeneuve, P. Hockett, M. J. J. Vrakking, and H. Niikura, *Coherent imaging of an attosecond electron wave packet*, Science **356**(6343), 1150 (2017).

[32] A. S. Kheifets and A. W. Bray, *RABBITT phase transition across the ionization threshold*, Phys. Rev. A **103**, L011101 (2021).

[33] A. Kheifets, *Revealing the target electronic structure with under-threshold RABBITT*, Atoms **9**(3), 66 (2021).